Pakistan Veterinary Journal

ISSN: 0253-8318 (PRINT), 2074-7764 (ONLINE)
DOI: 10.29261/pakvetj/2026.253

RESEARCH ARTICLE

# Ocular and Lacrimal Gland Involvement in Rabies: Histopathological and Molecular Evidence from Naturally Infected Animals

M. AKSOY[1]* and H. ERÖKSÜZ[2]

[1]Elazığ Veterinary Control Institute Directorate Rabies Diagnostic Laboratory, Elazığ, 23200, Türkiye; [2]University of Fırat, Faculty of Veterinary Medicine, Department of Pathology, Elazığ, 23119, Türkiye
*Corresponding author: mehmetaksoy933@gmail.com.tr

ARTICLE HISTORY (26-774)

Received: June 26, 2026
Revised: September 24, 2026
Accepted: September 28, 2026
Published online: October 19, 2026

**Key words:**
LN34 assay
Ocular tissues
Postmortem diagnosis
qRT-PCR
Rabies
Vitreous humor

**A B S T R A C T**

Rabies is still a fatal zoonosis, and post-mortem confirmation is mainly based on examination of brain tissue. However, collection of brain material may be difficult under field conditions and may pose a biosafety concern. We investigated ocular involvement in naturally infected animals by histopathology, immunohistochemistry, and molecular testing. Histopathology was conducted on 92 animals that tested positive for rabies via DFA. Ocular and lacrimal gland specimens (30 each) were independently selected for immunohistochemistry based on tissue availability, preservation, and adequacy to evaluate IL-6, IL-1β, TNFα, TLR3, TLR4, HSP70, CD3, and CD20. Molecular testing was performed on separate subsets of 50 fresh brain, 50 FFPE brain, and 50 vitreous humor samples selected based on specimen availability and analytical suitability. Typical lesions of rabies were observed, such as nonsuppurative meningoencephalitis, focal gliosis, and neuronal necrosis. There was no statistically significant difference in IL-6 positivity between ocular and lacrimal gland samples ($P>0.05$). HSP70 positivity was more frequent in lacrimal glands compared to ocular tissues (86.7% vs. 13.3%; $P<0.0001$), as was CD20 positivity (46.7% vs. 13.3%; $P=0.0029$). Rabies virus RNA was detected in 35/50 vitreous samples (70%) by LN34 qRT-PCR. The Ct values were generally higher in FFPE brain specimens than in fresh brain specimens. Detection of viral RNA in vitreous humor supports ocular involvement in centrifugal spread from the central nervous system. However, 15 samples of vitreous humor from DFA-positive animals were negative, suggesting that vitreous humor cannot be considered as an independent diagnostic specimen, but its potential role is supplementary and needs further evaluation.

**To Cite This Article:** Aksoy M and Eröksüz H, 2026. Ocular and lacrimal gland involvement in rabies: histopathological and molecular evidence from naturally infected animals. Pak Vet J, 46(10): 2499-2508. http://dx.doi.org/10.29261/pakvetj/2026.253

## INTRODUCTION

Rabies constitutes a zoonotic infection that is virtually always deadly after the onset of clinical symptoms and remains a critical public health issue in endemic areas, particularly where surveillance and laboratory capabilities are inadequate (Abela-Ridder *et al.*, 2018; World Health Organization, 2018; Afzal *et al.*, 2022). Infection exhibits a pronounced neurotropism, with the central nervous system (CNS) being the primary target, and laboratory verification is crucial as initial clinical symptoms are not distinctive for rabies (Fooks *et al.*, 2017; Chen *et al.*, 2025). Neuronal dysfunction during infection occurs together with host immune responses that may vary with the stage and distribution of infection (Guo *et al.*, 2019; Pan *et al.*, 2019; Yin *et al.*, 2021).

For postmortem confirmation, the direct fluorescent antibody (DFA) test performed on brain tissue remains a reference method (World Organisation for Animal Health, 2023). Brain sampling is not always straightforward, particularly when decomposition, restricted cranial access, or field logistics complicate specimen collection and handling (Banyard *et al.*, 2013). This has prompted interest in additional postmortem materials for molecular testing, not as replacements for validated brain-based diagnosis but as possible complementary specimens (Rupprecht *et al.*, 2018; Robardet *et al.*, 2021). The LN34 pan-lyssavirus qRT-PCR assay is one such molecular approach and has been evaluated in different specimen types (Gigante *et al.*, 2018; Condori *et al.*, 2020; Chierato *et al.*, 2024). More recently, the assay has

been modified through updated primer formulations and incorporation of an internal control into the single-well LN34M format (Gigante *et al.*, 2025).

Ocular tissues merit particular attention because of their anatomical and neural continuity with the CNS. Rabies-associated alterations have previously been described in retinal ganglion cells, structures related to the optic nerve, and lacrimal tissues (Jackson, 2016; Dalton *et al.*, 2020). By comparison, evidence on how often rabies virus RNA can be recovered from vitreous humor in naturally infected animals is scarce. Vitreous humor is a relatively protected ocular compartment, and examining it together with tissue lesions and immunohistochemical findings may help define the extent of ocular involvement during natural infection. Such an approach may also clarify whether vitreous humor has value as an additional postmortem specimen rather than as an alternative to brain tissue.

The study was therefore designed primarily to determine how frequently rabies virus RNA could be detected in vitreous humor from naturally infected animals using the LN34 qRT-PCR assay. We additionally delineated histopathological alterations in the eye, lacrimal gland, brain, and cerebellum; analyzed specific inflammatory and immune indicators in ocular and lacrimal gland tissues; and contrasted molecular identification in fresh and FFPE brain specimens while evaluating ocular materials as supplementary postmortem samples.

## MATERIALS AND METHODS

**Ethical Considerations:** The study was approved by the Animal Experiments Ethics Committee of the Elazığ Veterinary Control Institute (2021/04; 28 July 2021).

**Animals:** Specimens were collected from brain, cerebellum, eye, and lacrimal gland of the animals submitted to the Elazığ Veterinary Control Institute for routine rabies diagnosis in 2022 and 2023. In the present study, 92 animals (50 cattle, 23 dogs, 6 goats, 4 sheep, 3 donkeys, 2 horses, 2 foxes, 1 cat and 1 wolf) were examined and all were found to be positive for rabies by direct fluorescent antibody (DFA) test. Samples were obtained from naturally infected animals who died spontaneously or during quarantine/clinical observation; no experimental infection or euthanasia was conducted for study purposes.

**Histopathological examinations:** After DFA analysis, brain, cerebellum and lacrimal gland tissues were fixed in 10% neutral buffered formalin and eyes were fixed in Davidson's solution (Chidlow *et al.*, 2011). Paraffin embedded tissues were cut at 3–5µm and stained with hematoxylin and eosin (H&E) (Luna, 1968; Feldman and Wolfe, 2014). Sections (Olympus BX43, DP72) were independently evaluated by two pathologists blinded to case information and molecular data; differences were re-evaluated and, if necessary, reviewed by a third pathologist.

**Immunohistochemical examinations:** Thirty ocular and 30 lacrimal gland specimens were selected independently for immunohistochemistry according to tissue availability, preservation and suitability for serial sectioning. The sections were studied for TLR3, TLR4, IL-6, IL-1β, TNFα, HSP70, CD3 and CD20 by the streptavidin–biotin peroxidase method and PatoLab Anti-Polyvalent HRP Kit Table 1-A (Chidlow *et al.*, 2011). Antigen retrieval was performed with citrate solution and endogenous peroxidase was blocked. Slides were treated with primary antibodies for 1h at 37°C followed by biotinylated secondary antibody and streptavidin-horseradish peroxidase. Immunoreactivity was observed using AEC and Gill's hematoxylin counterstain. Staining was evaluated by a semi-quantitative histoscore which was computed as the product of the extent and intensity, and ranged from 0 to 2.7 (Table 1-B) (Carter *et al.*, 2004; Karabulut *et al.*, 2025). Positive controls and negative controls generated by omitting the main antibody were included.

**Table 1:** A. Antibody information. B. Immune score table. Table A. List of primary antibodies used in immunohistochemical analyses, host, and dilution ratio.

| Antibody | Manufacturer | Catalogue Numbers | Reactivity | Prediction |
|---|---|---|---|---|
| TLR3 | Affinity Biosciences | DF6415 | Human, Mouse, Rat | Bovine 100%, Horse 100%, Sheep 100% |
| TLR4 | Affinity Biosciences | AF7017 | Human, Mouse, Rat | Current product page does not provide veterinary prediction values |
| IL-6 | Affinity Biosciences | DF6087 | Human, Mouse, Rat | Bovine 100%, Dog 78%, Horse 71%, Sheep 71% |
| IL-1β | Affinity Biosciences | AF5103 | Human, Mouse, Rat | Horse 80%, Dog 70%b in the prediction model. |
| TNFα | Elabscience | ENT4689 | Human, Mouse, Rat | IHC is listed; I could not verify a manufacturer veterinary-species prediction for this catalogue. |
| HSP70 | Affinity Biosciences | AF5466 | Human, Mouse, Rat, Monkey | Bovine 100%, Sheep 100% |
| CD3 | Affinity Biosciences | DF6594 | Human, Mouse, Rat | Sheep 100%, Bovine 91%, Horse 91%, Dog 91% |
| CD20 | Affinity Biosciences | DF13319 | Human, Rat | Bovine 88%, Sheep 88%, Dog 88% |

All primary antibodies used in the immunohistochemical analyses were polyclonal antibodies raised in rabbit and were applied at a dilution of 1:100. Manufacturer-reported "Reactivity" represents the species listed for antibody use, whereas "Prediction" reflects sequence-based predicted cross-reactivity and should not be considered equivalent to species-specific IHC validation. Therefore, potential interspecies differences in antibody affinity cannot be excluded, and IHC findings were interpreted as tissue-level immunoreactivity rather than as quantitative interspecies comparisons.

**Table B:** Immunomohistochemical Scoring = Prevalence of Immunoreactivity × Severity of Immunoreactivity (Carter *et al.*, 2004).

| Prevalence of Immunoreactivity | Severity of Immunoreactivity |
|---|---|
| 0.1: Less than 25% | 0: None |
| 0.4: Between 26-50% | 0.5: Trace |
| 0.6: Between 51-75% | 1: Light |
| 0.9: Between 76-100% | 2: Moderate |
| | 3: Intense |

**Molecular analysis:** Molecular subsets were selected from DFA-positive cases according to specimen availability, preservation, and analytical suitability rather than formal random sampling. qRT-PCR was performed on 50 fresh brain/cerebellum, 50 FFPE brain, and 50 vitreous humor specimens. These represented separate analytical subsets and sample numbers therefore refer to specimens analyzed rather than additional animals. Vitreous humor

(approximately 1.0–1.5mL) was aseptically aspirated before brain manipulation and stored at −20°C. RNA was extracted from FFPE tissues using the RNeasy FFPE Kit (QIAGEN) and from fresh tissues and vitreous humor using the IndiSpin Pathogen Kit (INDICAL BIOSCIENCE).

Rabies virus RNA was detected using the LN34 pan-lyssavirus multiplex qRT-PCR assay with β-actin as an internal control and the QuantiNova Probe RT-PCR Kit (Table 2). Reactions (20µL) contained 17µL reaction mixture and 3µL RNA template and were run on a Rotor-Gene Q instrument: 45°C for 10 min, 95°C for 5 min, followed by 45 cycles of 94°C for 5 s and 56°C for 30s. Samples were tested in triplicate. Positive, extraction-negative, and no-template controls were included in each run. LN34 Ct<35 and β-actin Ct<33 were considered positive and valid, respectively (Wadhwa *et al.*, 2017; Gigante *et al.*, 2018; World Organisation for Animal Health, 2023).

**Table 2:** Primers and probes used in qRT-PCR (Wadhwa et al., 2017)

| PCR Type | Primer/Probe | Sequence (5'-3') | Position[a] |
|---|---|---|---|
| LN34 [c] | Probe LN34[b] | FAM-AA+C+ACCY+C+T+ACA+A+TGGA-BHQ1 | 59075 |
| | Probe LN34lago[b] | FAM-AA +C +ACTA +C +T +ACA +A +TGGA-BHQ1 | 59075 |
| | Primer forward1 | ACGCTTAACAACCAGATCAAAGAA | 1024 |
| | Primer forward2 | ACGCTTAACAACAAAATCADAGAAG | 1025 |
| | Primer reverse | CMGGGTAYTTRTAYTCATAYTGRTC | 1400164 |
| βactin primer and probe sequences used as internal controls | | | |
| βactin | βactin probe | (HEX)-TCCACCTTCCAGCAGATGTGGATCA-(BHQ1) | |
| | βactin forward | CGATGAAGATCAAGATCATTGC | |
| | βactin reverse | AAGCATTTGCGGTGGAC | |

qRT-PCR Primer/Probe Sequences. [a] Primer and probe positions are given relative to the Lyssavirus complete genome. [b] LNA-modified bases are indicated by a plus sign preceding the base in the sequence (e.g., +A, +G, +C, +T). [c] The pan-lyssavirus LN34 test has a mixed probe of Probe LN34 and Probe LN34lago in a 2:1 ratio, respectively; the forward primer is a 1:1 mixture of Primer forward1 and Primer forward2.

**Statistical analyses:** Statistical analysis was conducted using IBM SPSS Statistics v21. The Shapiro-Wilk and Bartlett tests were used to test normality and homogeneity of variances, respectively. Student's t-test was employed for comparison of normally distributed continuous data, and Pearson's chi-square or Fisher's exact test for categorical comparisons. The 95% CI for LN34-positive vitreous specimens was computed by the precise binomial (Clopper-Pearson) approach. $P<0.05$ was considered as statistically significant.

## RESULTS

**Macroscopic findings:** The brain commonly appeared edematous and congested. No gross lesions were observed in the eye or lacrimal gland tissues (Fig. 1).

**Microscopic findings:**

**Eye:** In addition to the inflammatory infiltrates observed in the retinal layers, Negri bodies were detected in the ganglion cells of the ganglion cell layer in 10/92 cases (10.9%) (Fig. 2).

**Lacrimal gland:** Histopathological lesions were observed in the lacrimal glands of 78/92 cases (84.8%). These lesions were characterized by inflammatory infiltrates composed of lymphocytes and a small number of plasma cells, predominantly in the interstitial areas and around the excretory ducts (Fig. 3).

**Brain:** Negri bodies were identified in several neuroanatomical regions, as summarised in Table 3. Nonsuppurative meningoencephalitis, focal gliosis, and neuronal necrosis in different regions of the brain were observed in all samples (Fig. 4).

**Cerebellum:** When cerebellar tissues from different rabies-positive animal species were examined, intracytoplasmic Negri bodies were observed in Purkinje cells in 2 horses (2/2), 2 donkeys (2/3), 3 sheep (3/4), 6 goats (6/6), 17 dogs (17/23), 1 wolf (1/1), 50 cattle (50/50), and 1 fox (1/2) (Table 3). Perivascular infiltrations around the meninges and blood vessels were notable in the affected cerebella (Fig. 5).

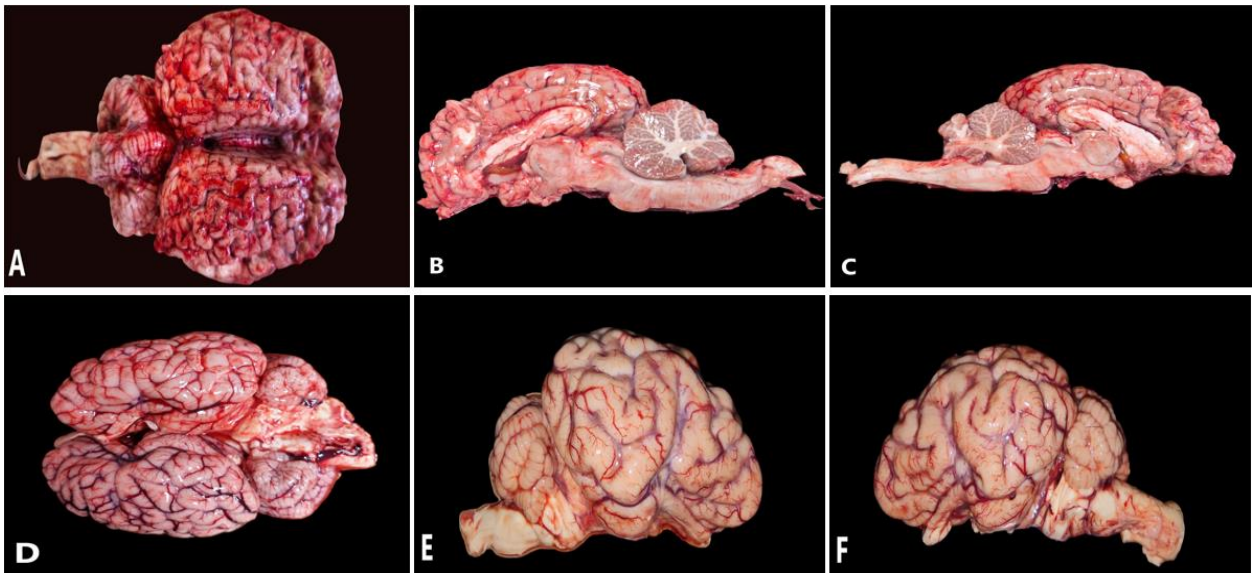



**Fig. 1:** Hemorrhagic, congested, and edematous appearance of the brain. A: Horse, B: Horse, C: Horse, D: Goat, E: Goat, F: Goat.

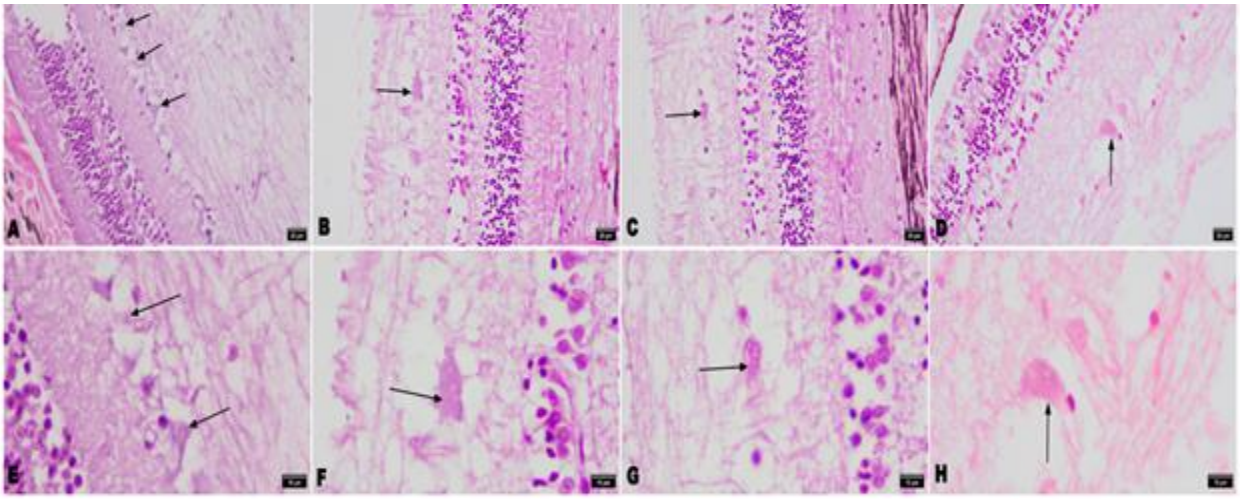


**Fig. 2:** Negri bodies within retinal ganglion cells (black arrows). A: Cattle, scale bar = 20 µm B: Dog, scale bar = 20 µm C: Dog, scale bar = 20 µm D: Goat, scale bar = 20 µm E: Cattle, scale bar = 10 µm F: Dog, scale bar = 10 µm G: Dog, scale bar = 10 µm H: Goat, scale bar = 10 µm.

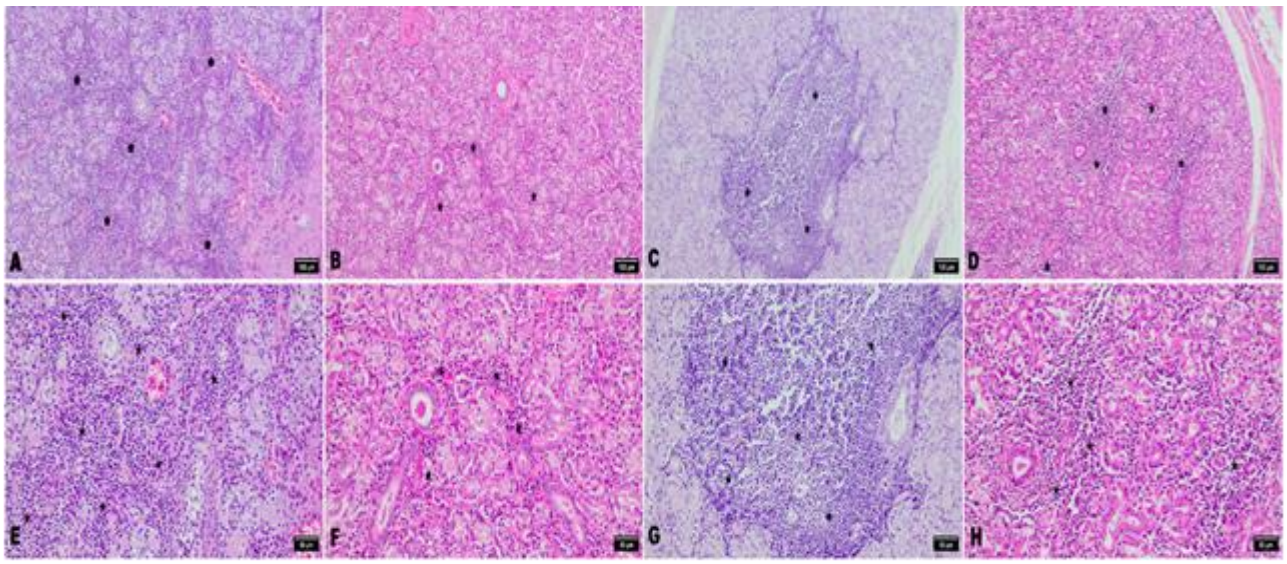


**Fig. 3:** Widespread lymphohistiocytic cell infiltration around the lacrimal ducts of different animal species (black star), H&E. A: Cattle, scale bar = 100 µm B: Goat, scale bar = 100 µm C: Dog, scale bar = 100 µm D: Sheep, scale bar = 100 µm E: Cattle, scale bar = 50 µm F: Goat, scale bar = 50 µm G: Dog, scale bar = 50 µm H: Sheep, scale bar = 50 µm.

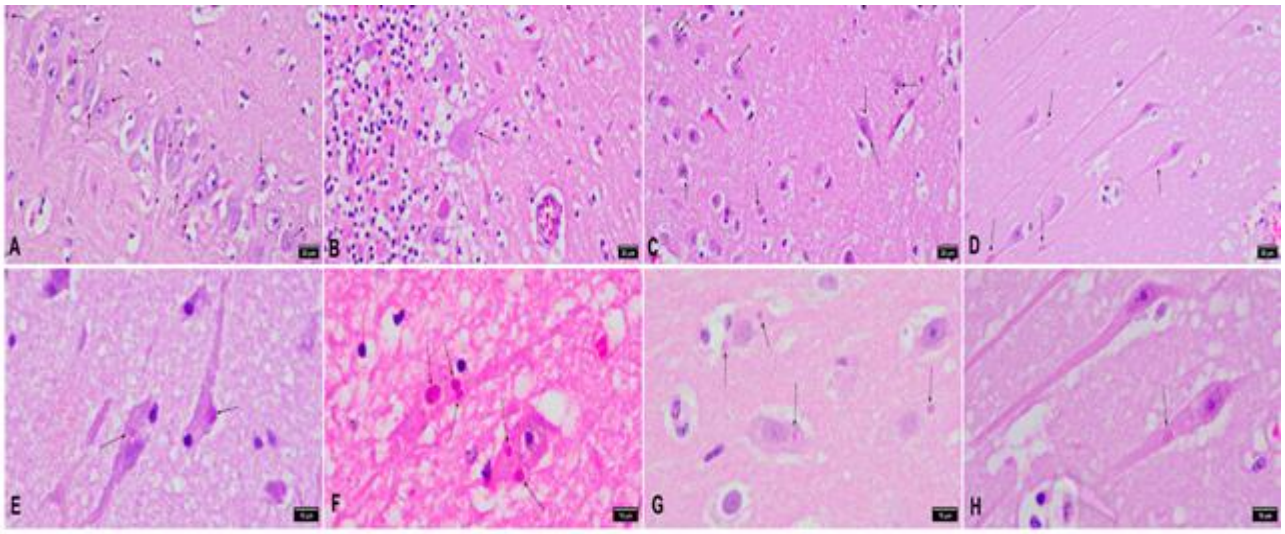


**Fig. 4:** Negri bodies (black arrows), H&E, in neurons in various brain regions of different animal species. A: Sheep, HC, scale bar = 20 µm B: Donkey, PO, scale bar = 20 µm C: Goat, CO, scale bar = 20 µm D: Cattle, HC, scale bar = 20 µm E: Dog, HC, scale bar = 10 µm F: Cattle, CP, scale bar = 10 µm G: Cattle, CO, scale bar = 10 µm H: Cattle, HC, scale bar = 10 µm.

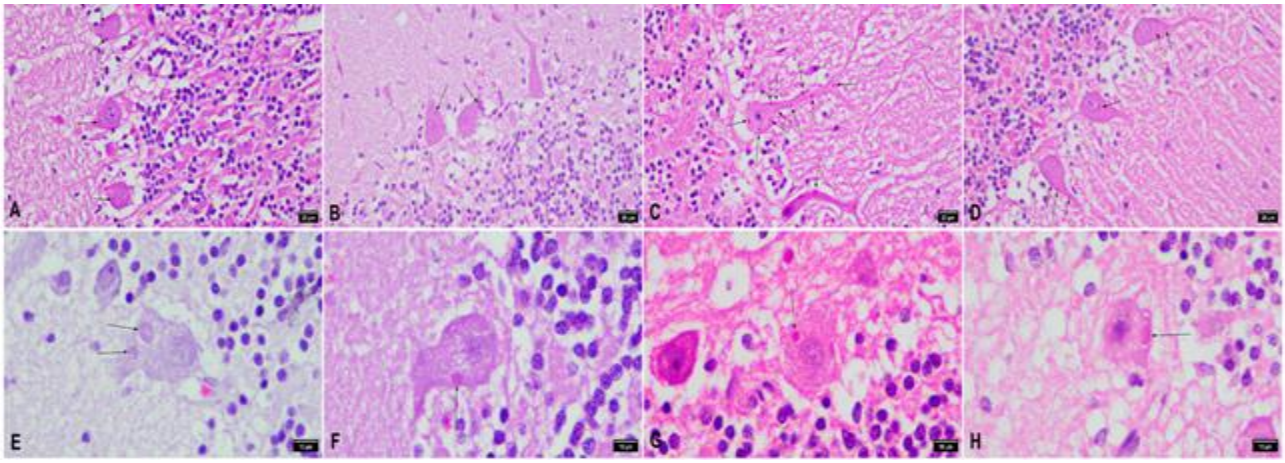



**Fig. 5:** Negri bodies (black arrows) in Purkinje cells of different animal species, H&E. A: Sheep, CE, scale bar = 20 µm B: Sheep, CE, scale bar = 20 µm C: Cattle, CE, scale bar = 20 µm D: Goat, CE, scale bar = 20 µm E: Dog, CE, scale bar = 10 µm F: Dog, CE, scale bar = 10 µm G: Dog, CE, scale bar = 10 µm H: Dog, CE, scale bar = 10 µm.

**Table 3:** Distribution of Negri bodies according to anatomical regions of the brain

| n | SPECIES | BO* | CE* | PO* | ME* | CO* | CP* | HC* | TA* | CF* |
|---|---|---|---|---|---|---|---|---|---|---|
| 2 | HORSE | 0 | 2 | 0 | 0 | 0 | 1 | 1 | 0 | 1 |
| 3 | DONKEY | 2 | 2 | 1 | 0 | 1 | 0 | 2 | 0 | 2 |
| 6 | GOAT | 3 | 6 | 1 | 0 | 3 | 1 | 5 | 0 | 4 |
| 1 | CAT | 0 | 0 | 0 | 0 | 1 | 0 | 1 | 0 | 1 |
| 4 | SHEEP | 0 | 3 | 0 | 0 | 4 | 0 | 3 | 0 | 3 |
| 23 | DOG | 1 | 17 | 1 | 0 | 1 | 0 | 17 | 0 | 1 |
| 1 | WOLF | 1 | 1 | 0 | 0 | 0 | 0 | 0 | 0 | 0 |
| 50 | COW | 15 | 50 | 3 | 1 | 25 | 24 | 31 | 5 | 19 |
| 2 | FOX | 0 | 1 | 0 | 0 | 0 | 0 | 2 | 0 | 0 |

*BO: Medulla oblongata; CE: Cerebellum; PO: Pons; ME: Midbrain; CO: Occipital lobe; CP: Parietal lobe; HC: Hippocampus; TA: Thalamus; CF: Frontal lobe; n: number of animals examined. A value of 0 indicates that the corresponding anatomical region was examined, but no Negri bodies were detected.

**Immunohistochemical findings:** Quantitative immunohistochemical scoring demonstrated that HSP70 and CD20 immunoreactivity were significantly higher in the lacrimal glands compared to the ocular tissues (P<0.0001 and P=0.0029, respectively). In contrast, IL-6 showed strong expression in both tissues, with little intertissue difference, whereas TLR3, TLR4, IL-1β, TNFα, and CD3 showed variable, generally low expression levels. The expression patterns of the investigated markers are described below. Table 4 presents the frequency of specimens showing immunoreactivity for each marker and the predominant tissue localization of staining, whereas the semi-quantitative IHC scores based on staining extent and intensity are presented separately in Fig. 6.

TLR3 immunoreactivity was absent in ocular tissues (0/30; 0%) but detected in lacrimal glands (5/30; 16.7%), predominantly in the acinar regions. TLR4 immunoreactivity was observed in ocular (7/30; 23.3%) and lacrimal gland tissues (6/30; 20.0%), mainly in the retinal inner nuclear layer and glandular acini, with no significant difference between tissues (P>0.05). IL-6 showed high positivity in both ocular (27/30; 90.0%) and lacrimal gland tissues (26/30; 86.7%), with staining throughout the retinal layers and glandular acini (P>0.05). IL-1β positivity was detected in 3/30 (10.0%) ocular and 3/30 (10.0%) lacrimal gland samples. In the positive specimens, immunoreactivity was localized throughout the retinal layers and within the glandular acini and excretory duct epithelium (P>0.05). TNFα immunoreactivity was observed in ocular (2/30; 6.7%) and lacrimal gland tissues (5/30; 16.7%), predominantly in the retinal nerve fiber layer and glandular acini. HSP70 positivity was detected in 4/30 (13.3%) ocular and 26/30 (86.7%) lacrimal gland samples, with significantly greater immunoreactivity in the lacrimal glands (P<0.0001). CD3 immunoreactivity was absent in ocular tissues and detected in one lacrimal gland sample (1/30; 3.3%). Staining was observed within the acinar region; however, because the cellular lineage of the positive cells was not independently confirmed, this finding was interpreted as regional CD3 immunoreactivity rather than definitive T-cell infiltration. CD20 immunoreactivity was detected in ocular (4/30; 13.3%) and lacrimal gland tissues (14/30; 46.7%), with significantly higher immunoreactivity in the lacrimal glands (P=0.0029); staining within retinal and lacrimal gland regions was not interpreted as definitive B-cell infiltration because the cellular origin of noncanonical staining was not independently confirmed.

**Table 4:** Frequency and predominant tissue localization of immunoreactivity for the investigated markers in ocular and lacrimal gland specimens.

| Marker | Eye (n = 30) Positive n (%) | Lacrimal gland (n = 30) Positive n (%) | Predominant tissue localization of immunoreactivity |
|---|---|---|---|
| TLR3 | 0 (0%) | 5 (16.7%) | Cytoplasmic (acinar cells) |
| TLR4 | 7 (23.3%) | 6 (20.0%) | Cytoplasmic/membranous |
| IL-6 | 27 (90.0%) | 26 (86.7%) | Cytoplasmic (retinal and acinar cells) |
| IL-1β | 3 (10.0%) | 3 (10.0%) | Cytoplasmic |
| TNF-α | 2 (6.7%) | 5 (16.7%) | Cytoplasmic |
| HSP70 | 4 (13.3%) | 26 (86.7%) | Cytoplasmic |
| CD3 | 0 (0%) | 1 (3.3%) | Lacrimal gland tissue region; cellular lineage not confirmed |
| CD20 | 4 (13.3%) | 14 (46.7%) | Retinal and lacrimal gland tissue regions; cellular lineage not confirmed |

Note*: Values are presented as the number and percentage of specimens showing immunoreactivity [positive n (%)]. The table summarizes the frequency of immunoreactive specimens and the predominant tissue localization of staining and does not represent semi-quantitative IHC scores. Semi-quantitative IHC scores, based on staining extent × intensity, are presented separately in Fig. 6.

**Molecular Findings:** The number of samples used in the molecular studies and the varying Ct values are shown in Fig. 7.

**Viral Nucleic Acid in the Vitreous Humor:** Rabies virus RNA was detected by qRT-PCR in 35/50 (70%) vitreous humour samples from DFA-positive animals, while 15/50 (30%) samples yielded negative results (Fig. 7).

**Viral Nucleic Acid in Fresh and FFPE Brain Tissues:** Rabies virus RNA was detected by LN34 qRT-PCR in all 50 fresh brain and all 50 FFPE brain tissue samples (50/50; 100% in both groups). β-actin amplification confirmed RNA integrity and amplification competence in the analyzed specimens and was used solely as an endogenous control. LN34 and β-actin Ct values are presented separately in Fig. 8.

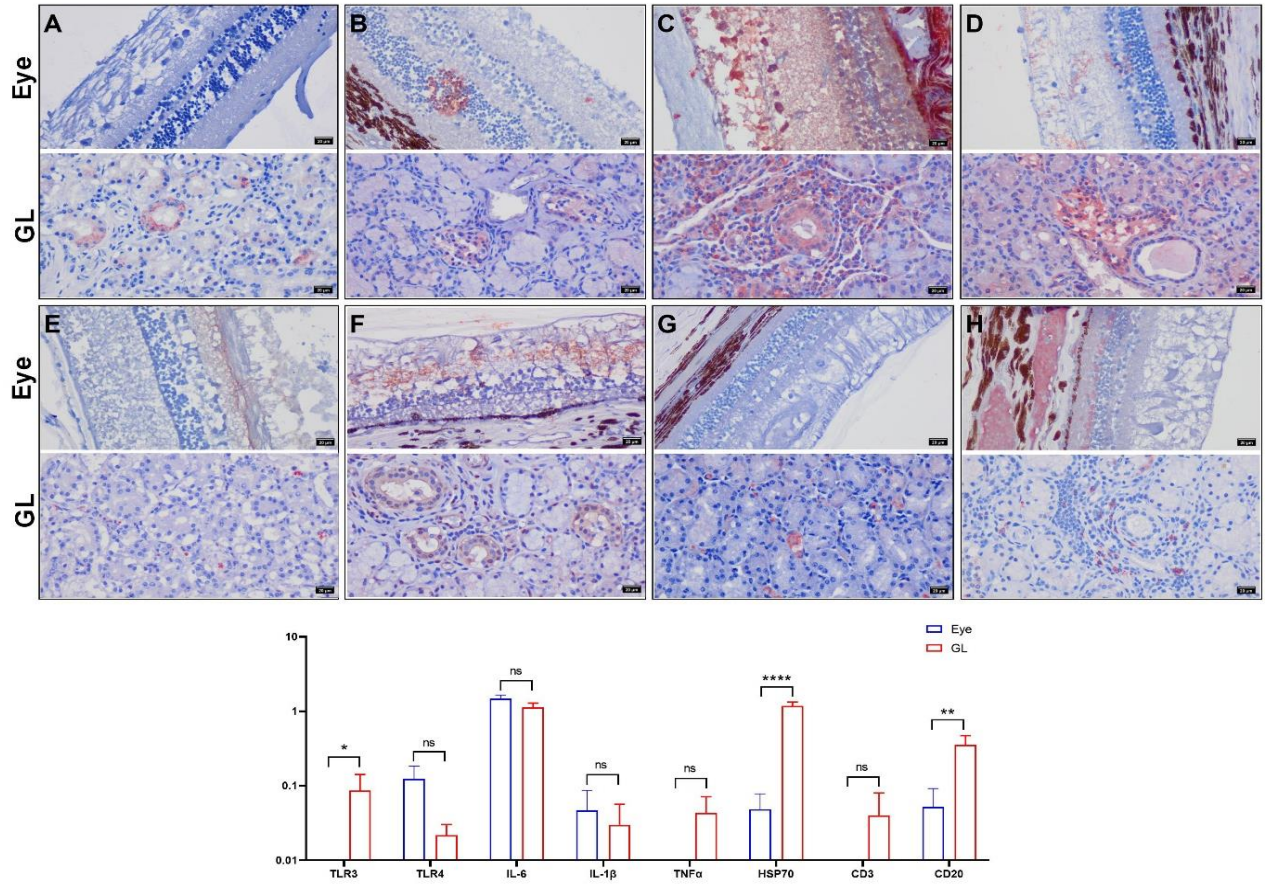



**Fig. 6:** A. TLR3 immunoreactivity. B. TLR4 immunoreactivity. C. IL-6 immunoreactivity. D. IL-1β immunoreactivity. E. TNFα immunoreactivity. F. HSP70 immunoreactivity. G. CD3 immunoreactivity. H. CD20 immunoreactivity. Comparative immunoreactivity scores in ocular and lacrimal gland tissues are presented as mean ± standard error (SEM). Statistical significance was evaluated using Student's t-test (scale bar = 20 µm; ×40) (ns: Not Significant).

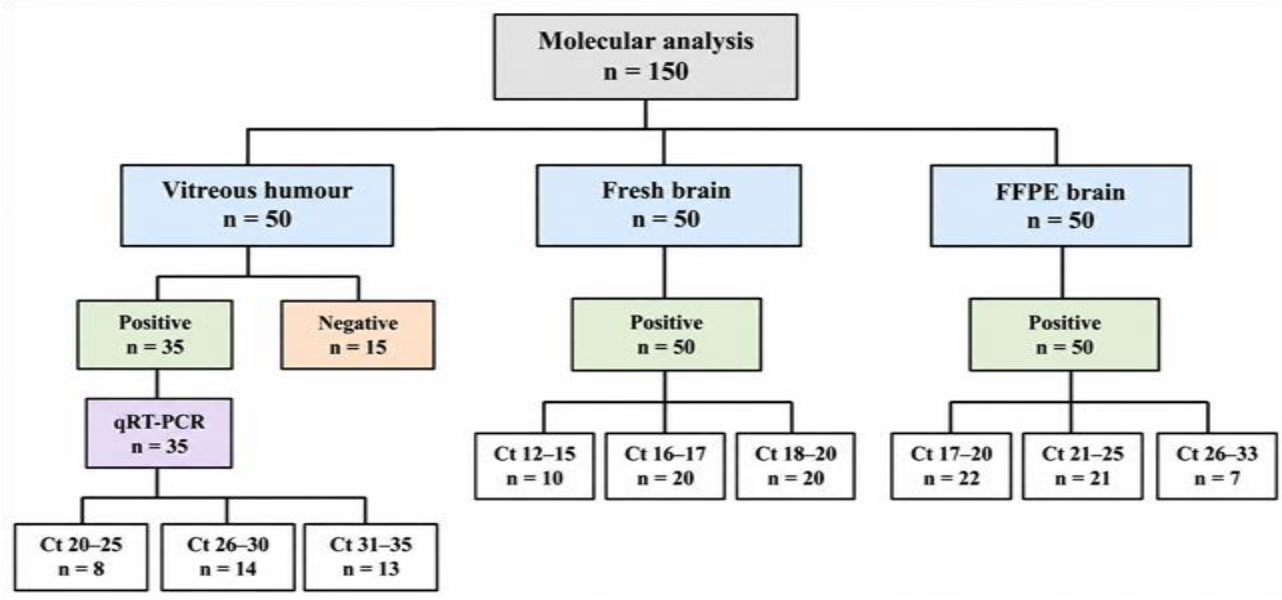



**Fig. 7:** Distribution of molecular results and LN34 Ct values according to specimen type. Molecular analysis included 50 vitreous humour, 50 fresh brain, and 50 FFPE brain specimens. Rabies virus RNA was detected in 35/50 vitreous humour specimens and in all fresh and FFPE brain specimens. Ct ranges and the corresponding numbers of positive specimens are shown for each sample type. Ct, cycle threshold; FFPE, formalin-fixed paraffin-embedded; qRT-PCR, quantitative reverse transcription polymerase chain reaction.

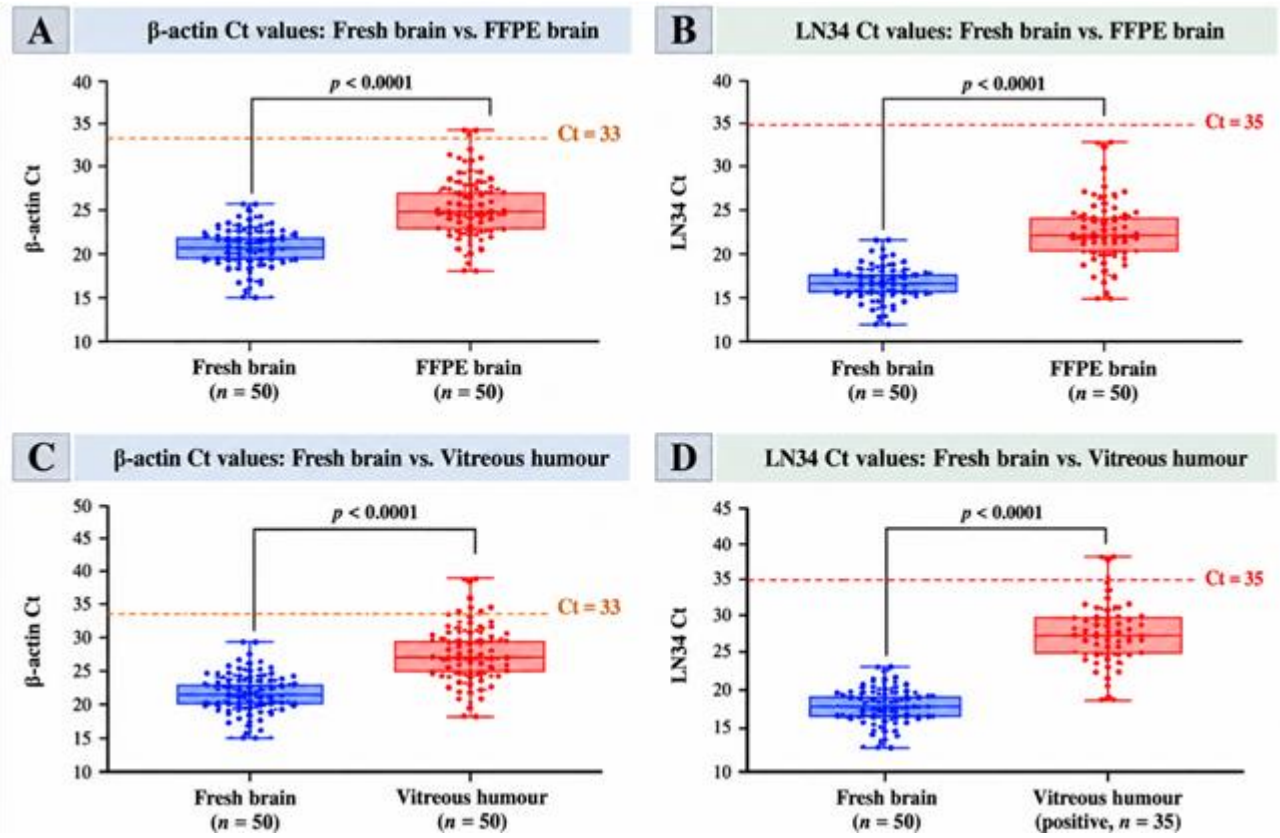



**Fig. 8:** Distribution of β-actin and LN34 Ct values among fresh brain, FFPE brain, and vitreous humour specimens from DFA-positive animals. (A) β-actin Ct values in fresh brain and FFPE brain specimens (n=50 each). (B) LN34 Ct values in fresh brain and FFPE brain specimens (n=50 each). (C) β-actin Ct values in fresh brain and vitreous humour specimens (n=50 each). (D) LN34 Ct values in fresh brain (n=50) and LN34-positive vitreous humour specimens (n=35). β-actin was evaluated solely as an endogenous control for RNA integrity and amplification performance and was not used to normalize LN34 Ct values. Dashed lines indicate the predefined Ct thresholds for β-actin (Ct=33) and LN34 (Ct=35). Ct, cycle threshold; FFPE, formalin-fixed paraffin-embedded.

## DISCUSSION

Rabies remains almost uniformly fatal once clinical signs develop, and postmortem confirmation still relies principally on CNS tissue, especially brain (Yaz, 2025; Pardeshi *et al.*, 2026). After peripheral replication, rabies virus reaches the CNS by retrograde axonal transport and subsequently disseminates centrifugally to peripheral tissues (Guo *et al.*, 2019; Scott and Nel, 2021; Sharma *et al.*, 2023). In this context, our most significant finding was the identification of rabies virus RNA in 35 out of 50 vitreous samples (70%). This molecular discovery coincided with histopathological alterations in ocular and lacrimal gland tissues, as well as unique immunohistochemical profiles, featuring prevalent IL-6 positivity in both tissues and significantly elevated HSP70 and CD20 positivity in the lacrimal gland. All fresh and FFPE brain samples exhibited positivity for LN34. The vitreous observations consequently provide molecular proof of eye involvement during natural infection; however, the 15 negative vitreous samples illustrate why this material cannot be assessed without reference to established brain-based diagnoses.

Histological lesions in the CNS including neuronal degeneration, gliosis and perivascular and lymphocytic infiltrates are consistent with the known histopathological features of rabies encephalitis and are comparable with findings reported in naturally infected animals of diverse species (Bassuino *et al.*, 2016; Achkar *et al.*, 2019; Markbordee *et al.*, 2024). Negri bodies were not limited to one neuroanatomical site and showed variable distribution among the cases. This heterogeneity is consistent with previous findings and warns against the assumption of uniform tissue distribution in natural infection (Markbordee *et al.*, 2024). Ocular findings extend this picture beyond the CNS. Degeneration and inclusions in retinal ganglion cells are compatible with involvement of the optic pathway (Guo *et al.*, 2019; Dalton *et al.*, 2020), whereas lymphohistiocytic infiltrates in the lacrimal gland indicate a local inflammatory response within this peripheral tissue.

Immunohistochemically, immunoreactivity for the proinflammatory cytokines IL-6, IL-1β, and TNFα suggests that neuronal damage in rabies infection may be associated not only with the direct effects of the virus but also with the host immune response (Farahtaj *et al.*, 2019; Kiflu, 2024). The inflammatory and immune responses observed in ocular and lacrimal tissues may reflect local manifestations of the broader host-response mechanisms previously described in rabies-infected nervous tissues (Pan *et al.*, 2019). The increase in IL-6 observed in the ocular and lacrimal gland tissues is consistent with the activation of the innate immune response and is associated with the ability of rabies virus to modulate the host immune response (Pan *et al.*, 2019; Yin *et al.*, 2021). However, it has been reported that this cytokine response is part of a complex immune regulatory process that influences the course of the disease, and that the rabies virus, in particular,

can limit the immune response by suppressing interferon signaling pathways (Kiflu, 2024; Chen *et al.*, 2025). The observed immunoreactivity of HSP70 and Toll-like receptors may reflect inflammatory and cellular stress responses associated with rabies infection ; however, the present findings do not establish direct activation of specific signalling pathways or a causal relationship with viral replication.

CD3 and CD20 are routinely used as markers of T- and B-lymphocyte lineages, but their interpretation becomes less secure when staining is cytoplasmic, atypical, or occurs outside the expected cellular pattern (Oliveira *et al.*, 2012; Ferry, 2018; Pan *et al.*, 2018; Cho, 2022). CD20 immunoreactivity was more frequent in lacrimal gland than in ocular tissue in our material. We did not, however, confirm the lineage of the stained cells in retinal or acinar regions with additional markers. For this reason, the CD20 signal was not taken as direct evidence of B-cell infiltration, and the sparse CD3 staining was interpreted with the same caution. Confirming the cellular source of these signals will require additional lineage markers or multiplex methods.

While Dalton *et al.* (2020) demonstrated ocular and lacrimal gland lesions in naturally occurring rabies, this study expands on these observations by integrating histopathological, immunohistochemical, and molecular findings in the same tissues of naturally infected animals. In addition to confirming ocular and lacrimal gland involvement, this study demonstrated LN34-detectable rabies virus RNA in vitreous humor and provided molecular evidence of viral RNA distribution within ocular compartments.

A principal finding of this study is that viral RNA can be detected at a significant frequency in the vitreous fluid. The LN34 pan-lyssavirus qRT-PCR assay has a high analytical sensitivity allowing reliable detection in different types of samples (Gigante *et al.*, 2018; Dettinger *et al.*, 2022). With a positivity rate of 70% in vitreous samples (35/50; 95% CI: 55.4-82.1%) this study demonstrates that rabies virus RNA can be detected with significant frequency in this compartment. This is in line with previous studies that have reported the detection of viral presence in the peripheral and neurally connected tissues (Sharma *et al.*, 2023). However, the wide distribution of Ct values and the finding of negative cases suggest that vitreous fluid is not a biological matrix that accurately represents viral burden, but rather a biological matrix indicating the presence of viral RNA. This finding is supportive of the concept that ocular compartments may serve as indicators of viral dissemination, not as primary sites of viral replication. Such interpretation is in agreement with the high neurotropism of rabies virus and its capacity to move along neuronal pathways with structural changes in infected neural tissues (Guo *et al.*, 2019). In other viral infections, low titers, dilution and transmission dynamics have also been documented to impact detection of virus in ocular fluids (Bayyoud *et al.*, 2020; Casagrande *et al.*, 2020; Bayyoud *et al.*, 2021; Tieger *et al.*, 2022).

While vitreous data do not support replacing brain-based diagnosis, they do support the practical value of vitreous fluid as a complementary sample, especially when access to the skull is limited or postmortem conditions are suboptimal. Dalton *et al.* (2020) studied ocular and lacrimal gland involvement in 18 naturally infected animals. Our study extends these findings by histopathological examination of a larger cohort of 92 animals, immunohistochemical analysis of selected specimens, and qRT-PCR testing of vitreous humor from 50 animals. Rabies virus RNA has been detected in postmortem vitreous fluid from a human case (Centers for Disease Control and Prevention, 1997), but the present study extends this to naturally infected animals with RNA detected in 35 of 50 vitreous samples (70%). These results indicate that vitreous humor can be a site where viral RNA can be detected during natural infection with rabies. The diagnostic reliability of this finding is limited by the variable Ct values and by the fact that 15 samples were negative.

Higher Ct values obtained in molecular analysis of formalin-fixed, paraffin-embedded (FFPE) tissues are consistent with degradation of RNA integrity by formalin fixation (Condori *et al.*, 2020; Dalton *et al.*, 2020). However, a loss of sensitivity compared to fresh tissues is expected, although the LN34 assay targeting short amplicons partially circumvents this drawback (Condori *et al.*, 2020). These results show that the evaluation of molecular methods in parallel with immunohistochemistry and histopathology provides complementary molecular and pathological information, especially in suboptimal samples.

These data should be interpreted in light of several limitations. Because the study included only DFA-positive animals, diagnostic specificity and false-positive rates could not be estimated in the absence of rabies-negative biological controls. Technical controls confirmed assay performance but do not substitute for negative animals. The multispecies design also introduced biological heterogeneity, with several species represented by small numbers, precluding meaningful comparisons at the species level. Immunohistochemical and molecular specimens were selected for availability and analytical suitability, rather than by random sampling, which could have led to selection bias and reduced comparability among subsets. Furthermore, the antibodies were not independently validated in all the species investigated and the staining patterns might have been affected by differences in cross-reactivity. Postmortem interval, transport and vitreous collection conditions were not uniform and may have affected RNA preservation. Because no virus isolation or infectivity assay was performed, RNA detection in vitreous humor should not be interpreted as evidence of infectious virus or transmission risk. Finally, β-actin served as an internal control, but its use for quantitative normalization across fresh brain, FFPE brain, and vitreous specimens was not validated; consequently, LN34/β-actin Ct ratios should not be regarded as measures of relative viral load.

**Conclusions:** Brain tissue examined by DFA remains the reference standard for postmortem rabies diagnosis. In the present series, rabies virus RNA was also found in vitreous humor, supporting involvement of this ocular compartment during natural infection and remaining consistent with centrifugal dissemination from the CNS. Rabies virus RNA was not detectable in every vitreous sample from DFA-positive animals. Vitreous humor therefore should not be used as a standalone diagnostic specimen. Its usefulness is

more appropriately investigated as a complementary material for molecular examination of rabies. Overall, LN34 qRT-PCR detected rabies virus RNA in 35 of 50 (70%) vitreous samples, whereas 15 samples were negative. Future studies that include rabies-negative animals, standardized collection procedures, and larger cohorts are needed to determine how consistently vitreous RNA detection reflects ocular involvement and whether it has practical value in postmortem rabies investigation.

**Acknowledgment:** This study was derived from the PhD thesis of Mehmet AKSOY, titled 'Histopathological, Immunohistochemical, and Molecular Investigation of the Eye, Lacrimal Gland, and Optic Nerve in Animals Infected with Natural Rabies Virus', under the supervision of Prof. Dr. Hatice ERÖKSÜZ at Fırat University. The authors also thank the Fırat University Scientific Research Projects Coordination Unit (FÜBAP) for financial support under Project No. 2023-VF-23-13. Views and opinions expressed are however those of the author(s) only and do not necessarily reflect those of the Republic of Türkiye Ministry of Agriculture and Forestry. Neither the Republic of Türkiye Ministry of Agriculture and Forestry can be held responsible for them.

**Authors contributions:** MA, HE: Designed and structured the study. MA: Collected tissue and data, performed histopathological, immunohistochemical and molecular analyses. MA, HE: Data interpretation, data analysis and consistent analysis. MA: Writing - Original draft. All authors contributed to the article and approved the final version.

**Financial support:** This research was funded by the Fırat University Scientific Research Projects Coordination Office (2023-VF-23-13).

## REFERENCES

Abela-Ridder B, Kessels J, Dieuzy-Labaye I, *et al*., 2018. Global rabies control: the role of international organisations and the Global Strategic Plan to eliminate dog-mediated human rabies. Revue Scientifique Et Technique 37:741-49.

Achkar SM, Fernandes ER, Guedes F, *et al*., 2019. In situ histopathological and immunohistochemical characterization of rabies in the brains of naturally infected equines and bovines. Brazilian Journal of Veterinary Medicine 41:e101419-e19.

Afzal S, Nasir M, Bhaya MN, *et al*., 2022. Multifactorial Complexity and Zoonotic Aspects of Dog-Mediated Human Rabies in Pakistan. Pakistan Veterinary Journal 42:445-52.

Banyard AC, Horton DL, Freuling C, *et al*., 2013. Control and prevention of canine rabies: the need for building laboratory-based surveillance capacity. Antiviral Research 98:357-64.

Bassuino DM, Konradt G, Cruz RA, *et al*., 2016. Characterization of spinal cord lesions in cattle and horses with rabies: the importance of correct sampling. Journal of Veterinary Diagnostic Investigation 28:455-60.

Bayyoud T, Iftner A, Iftner T, *et al*., 2020. Absence of severe acute respiratory syndrome coronavirus 2 RNA in ocular tissues. American Journal of Ophthalmology Case Reports 19:100805.

Bayyoud T, Iftner A, Iftner T, *et al*., 2021. Severe acute respiratory syndrome coronavirus 2: Can it be detected in the retina? PLoS One 16:e0251682.

Carter JH, Douglass LE, Deddens JA, *et al*., 2004. Pak-1 expression increases with progression of colorectal carcinomas to metastasis. Clinical Cancer Research 10:3448-56.

Casagrande M, Fitzek A, Püschel K, *et al*., 2020. Detection of SARS-CoV-2 in human retinal biopsies of deceased COVID-19 patients. Ocular Immunology and Inflammation 28:721-25.

Centers for Disease Control and Prevention, 1997. Human rabies-Kentucky and Montana, 1996. Morbidity and Mortality Weekly Report 46:397-400.

Chen SJ, Rai CI, Wang S-C, *et al*., 2025. Infection and prevention of rabies viruses. Microorganisms 13:380.

Chidlow G, Daymon M, Wood JPM, *et al*., 2011. Localization of a wide-ranging panel of antigens in the rat retina by immunohistochemistry: comparison of Davidson's solution and formalin as fixatives. Journal of Histochemistry & Cytochemistry 59:884-98.

Chierato MER, Silveira VBV, Pavani D, *et al*., 2024. Evaluation of LN34 Pan-Lyssavirus RT-qPCR assay for rabies diagnosis in Brazil. Journal of Virological Methods 327:114948.

Cho J, 2022. Basic immunohistochemistry for lymphoma diagnosis. Blood Research 57:55-61.

Condori RE, Niezgoda M, Lopez G, *et al*., 2020. Using the LN34 pan-lyssavirus real-time RT-PCR assay for rabies diagnosis and rapid genetic typing from formalin-fixed human brain tissue. Viruses 12:120.

Dalton MF, Siepker CL, Maboni G, *et al*., 2020. Ocular and lacrimal gland lesions in naturally occurring rabies of domestic and wild mammals. Veterinary Pathology 57:409-17.

Dettinger L, Gigante CM, Sellard M, *et al*., 2022. Detection of apparent early rabies infection by LN34 pan-lyssavirus real-time RT-PCR assay in Pennsylvania. Viruses 14:1845.

Farahtaj F, Alizadeh L, Gholami A, *et al*., 2019. Natural infection with rabies virus: a histopathological and immunohistochemical study of human brains. Osong Public Health Research Perspectives 10:6.

Feldman AT and Wolfe D, 2014. Tissue processing and hematoxylin and eosin staining. In: Day, C. (eds) Histopathology. Methods in Molecular Biology, vol 1180. Humana Press, New York, NY. pp 31-43. https://doi.org/10.1007/978-1-4939-1050-2_3.

Ferry JA, 2018. There are no magic bullets in hematopathology: even immunostains for CD20 and CD3 can get you into trouble. Advances in Anatomic Pathology 25:14-23.

Fooks AR, Cliquet F, Finke S, *et al*., 2017. Rabies. Nature Reviews Disease Primers 3:17091.

Gigante CM, Dettinger L, Powell JW, *et al*., 2018. Multi-site evaluation of the LN34 pan-lyssavirus real-time RT-PCR assay for post-mortem rabies diagnostics. PLoS One 13:e0197074.

Gigante CM, Wicker V, Wilkins K, *et al*., 2025. Optimization of pan-lyssavirus LN34 assay for streamlined rabies diagnostics by real-time RT-PCR. Journal of Virological Methods 333:115070.

Guo Y, Ahmad W, Song Y, *et al*., 2019. In vitro infection of street and fixed rabies virus strains inhibit gene expression of actin-microtubule binding proteins EB3 and p140cap in Neurons. Pakistan Veterinary Journal 39:359-64.

Jackson AC, 2016. Human rabies: a 2016 update. Current Infectious Disease Reports 18:1-6.

Karabulut B, Eroksuz H, Eroksuz Y, *et al*., 2025. Exploring minocycline's effect on retinal degeneration following N-methyl-N-nitrosourea exposure in rats. Veterinary Medicina (Praha) 70:247.

Kiflu AB, 2024. The immune escape strategy of rabies virus and its pathogenicity mechanisms. Viruses 16:1774.

Luna LG (ed) 1968. Manual of Histologic Staining Methods of the Armed Forces Institute of Pathology. 3rd Ed, Blakiston Division, McGraw-Hill, New York, USA.

Markbordee B, Iamohbhars N, Shiwa-Sudo N, *et al*., 2024. Histopathological and immunohistochemical examination of the brains of rabid dogs in the Philippines. Journal of Veterinary Medical Science 86:1243-51.

Oliveira JL, Grogg KL, Macon WR, *et al*., 2012. Clinicopathologic features of B-cell lineage neoplasms with aberrant expression of CD3: a study of 21 cases. The American Journal of Surgical Pathology 36:1364-70.

Pan Y, Xie LJ, Wei XK, *et al*., 2019. Differential Expression Analysis of microRNA in the Central Nervous System of Mouse Infected with Rabies Virus. Pakistan Veterinary Journal 39:49-55.

Pan Z, Chen M, Zhang Q, *et al*., 2018. CD3-positive plasmablastic B-cell neoplasms: a diagnostic pitfall. Modern Pathology 31:718-31

Pardeshi G, Sharma P and Ittiel A, 2026. Rabies post-exposure prophylaxis in India: a SWOT analysis. Therapeutic Advances in Vaccines and Immunotherapy 14:25151355251410780.

Robardet E, Servat A, Rieder J, *et al*., 2021. Multi-annual performance evaluation of laboratories in post-mortem diagnosis of animal rabies: Which techniques lead to the most reliable results in practice? PLoS Neglected Tropical Diseases 15:e0009111.

Rupprecht CE, Fooks AR and Abela-Ridder B (eds), 2018. Laboratory techniques in rabies. 5th Ed, World Health Organization, Geneva, Switzerland.

Scott TP and Nel LH, 2021. Lyssaviruses and the fatal encephalitic disease rabies. Frontiers in Immunology 12:786953.

Sharma AK, Prashar P, Bharti OK, *et al.*, 2023. Diagnosis of rabies using reverse-transcription polymerase chain reaction on post-mortem skin tissue specimens of the nasolabial plate in a rabies suspected cow: a case study. Journal of Veterinary Medical Science 85:844-48.

Tieger M, Das Adhikari U, Mukai S, *et al.*, 2022. SARS-CoV-2 RNA detected in vitreous samples obtained at autopsy. Journal of VitreoRetinal Diseases 6:183-87.

Wadhwa A, Wilkins K, Gao J, *et al.*, 2017. A pan-lyssavirus taqman real-time RT-PCR assay for the detection of highly variable rabies virus and other lyssaviruses. PLoS Neglected Tropical Diseases 11:e0005258.

World Health Organization, 2018. WHO Expert Consultation on Rabies: Third Report. WHO Technical Report Series No. 1012, World Health Organization, Geneva, Switzerland.

World Organisation for Animal Health, 2023. Rabies (infection with rabies virus and other lyssaviruses). In: Manual of Diagnostic Tests and Vaccines for Terrestrial Animals. 13th ed, World Organisation for Animal Health (WOAH), Paris, France, pp:1-38.

Yaz AK, 2025. Rabies Virus: A review of pathogenesis, diagnosis, and prevention. Academic International Journal of Veterinary Medicine 3:28-42.

Yin J, Wang X, Mao R, *et al.*, 2021. Research advances on the interactions between rabies virus structural proteins and host target cells: Accrued knowledge from the application of reverse genetics systems. Viruses 13:2288.